Observed Spatial Characteristics of Beijing Urban Climate Impacts on Summer Thunderstorms

JINGJING DOU

Institute of Urban Meteorology, China Meteorological Administration, and Chinese Academy of Meteorological Sciences, Beijing, China

YINGCHUN WANG

Beijing Meteorological Service, Beijing, China

ROBERT BORNSTEIN

Institute of Urban Meteorology, China Meteorological Administration, Beijing, China, and Department of Meteorology and Climatology, San Jose State University, San Jose, California

SHIGUANG MIAO

Institute of Urban Meteorology, China Meteorological Administration, Beijing, China

(Manuscript received 21 November 2013, in final form 28 August 2014)

ABSTRACT

This study investigates interactive effects from the Beijing urban area on temperature, humidity, wind speed and direction, and precipitation by use of hourly automatic weather station data from June to August 2008–12. Results show the Beijing summer urban heat island (UHI) as a multicenter distribution (corresponding to underlying land-use features), with stronger nighttime than daytime values (averages of 1.7° vs 0.8°C, respectively). Specific humidity was lower in urban Beijing than in surrounding nonurban areas, and this urban dry island is stronger during day than night (maximum of -2.4 vs $-1.9\,g\,kg^{-1}$). Wind direction is affected by both a mountain–valley-breeze circulation and by urbanization. Morning low-level flows converged into the strong UHI, but afternoon and evening southerly winds were bifurcated by an urban building-barrier-induced divergence. Summer thunderstorms also thus bifurcated and bypassed the urban center because of the building-barrier effect during both daytime and nighttime weak-UHI (<1.25°C) periods. This produced a regional-normalized rainfall (NR) minimum in the urban center and directly downwind of the urban area (of up to −35%), with maximum values along its downwind lateral edges (of >15%). Strong UHIs (>1.25°C), however, induced or enhanced thunderstorm formation (again day and night), which produced an NR maximum in the most urbanized area of up to 75%.

1. Introduction

Urbanization has rapidly spread globally during the last decades (e.g., Seto et al. 2011). This process modifies surface characteristics and the energy and moisture balances of both underlying surfaces and the lower atmosphere, which drives formation of distinct local urban climates (e.g., Yang et al. 2013a,b). These urban impacts thus modify urban temperatures, specific humidity, wind speed, and precipitation values, which either increase or decrease (relative to those in surrounding rural areas), depending on which urban modifications dominate at a given moment.

a. Urban climate

Structural and land-cover differences between urban and rural areas, as well as anthropogenic heat sources and aerosol layers, can produce urban 2-m temperatures warmer than those over surrounding rural regions (e.g.,

Denotes Open Access content.

Corresponding author address: Shiguang Miao, IUM/CMA, No. 55 Beiwaxili Road, Haidian District, Beijing, 100089, China.
E-mail: sgmiao@ium.cn

DOI: 10.1175/JAMC-D-13-0355.1

Bornstein 1968; Stewart and Oke 2012). This difference between urban and rural stations was first observed by Howard (1833) in London and is referred to as an urban heat island (UHI). Conversely, urban cool islands (UCIs) can also form, for example, though local shading effects.

Both UCIs and UHIs have been observed in more than 1000 cities throughout the world (Magee et al. 1999). Their spatial and temporal characteristics have been extensively documented (e.g., Manley 1958; Garstang et al. 1975; Landsberg 1981; Ripley et al. 1996; Jauregui 1997; Brazel et al. 2000; Kim and Baik 2005; Jin et al. 2005).

Temperature observations in a variety of climate regimes by Imamura (1991) showed that rural soil-moisture content controlled whether UHIs or UCIs formed at a given site during a specific season. The reason for this behavior is that urban areas cool more slowly at night and warm more slowly during daytime hours than do areas with dry rural soils; the reverse is true in areas with wet rural soils (Swaid 1991). This concept was used to relate UHI impacts on regional global warming in a variety of climates by Bornstein et al. (2012), while Georgescu et al. (2011, 2012) drew similar conclusions based on numerical simulations.

Relative humidity excesses and deficits in urban areas have also been examined by many researchers (e.g., Unkašević et al. 2001). These authors delineated mechanisms by which urban areas can produce urban moist islands, for example, moisture from winter and nighttime combustion, urban snowmelt with rural temperatures below freezing (Hage 1975), and higher rural dewfall rates (Ackerman 1971). Reduced evaporation from asphalt and concrete surfaces during daytime hours, conversely, produces urban dry islands (UDIs; Clark et al. 1985).

Urbanization also affects 10-m wind speed and direction, for example, urban buildings increase surface roughness length z_0 values (Oke 1987), increasing frictional drag over a city. Bornstein and Johnson (1977) found New York City (NYC), New York, thus reduces regional speeds when they are $> 4\,\mathrm{m\,s^{-1}}$, while well-developed UHIs caused urban speeds to accelerate with regional speeds less than that value. UHI-induced circulations also modify wind directions; for example, Fujibe (2003) demonstrated that the Tokyo, Japan, UHI causes convergence into the city during warm-season afternoons.

Long-term summer convective precipitation data from St. Louis, Missouri, and other U.S. urban areas were analyzed by Huff and Changnon (1972, 1973), who found downwind urban enhancement. Similar results were found by Shepherd et al. (2002) from analysis of warm-season precipitation around Atlanta, Georgia, during 1998–2000 by use of Tropical Rainfall Measuring Mission (TRMM) satellite-borne radar observations. Burian and Shepherd (2005) used data from 19 rain gauges within and near Houston to show that its warm reason rainfall increased by 25% from 1940–58 to 1984–99.

A modeling case study simulation by Hjelmfelt (1982) showed increased warm-season upward motion downwind of St. Louis, while the Fifth-generation Pennsylvania State University–National Center for Atmospheric Research (NCAR) Mesoscale Model (MM5) simulations by Craig and Bornstein (2002) of an Atlanta thunderstorm showed its formation caused by UHI-induced convergence, as the rainfall was centered over the city and because a second simulation without the city did not produce the event. Simulations of two thunderstorms over Atlanta with the Weather Research and Forecasting (WRF) Model by Shem and Shepherd (2009) also showed the convergence effect, but with rainfall increased downwind of the city, as a weak background flow existed.

To reconcile the above conflicting precipitation results, climatological analyses by Bornstein and LeRoy (1990) for NYC (over two summers) and by Bornstein and Lin (2000) for Atlanta (six events during the two-week-long 1996 Olympics) showed that, while UHIs initiate convective activity over cities during nearly calm regional flow [also found over London by Atkinson (1985)], moving thunderstorms can bifurcate and move around cities because of a building-barrier effect (thus producing minimum precipitation over cities and maxima around them and in their downwind reconvergence area). This synthesis–hypothesis by Bornstein (2011) is thus consistent with the downwind urban-edge maximum precipitation effect noted in previous studies, but it differentiates the two conflicting urban thermodynamic impacts on precipitation.

The review of Shepherd (2005) of urban precipitation studies from 1990 to 2005 also only mostly addressed urban thermodynamic effects, while only briefly discussing aerosol impacts. TRMM satellite data, however, were used by Rosenfeld (2000) to show that giant cloud condensation nuclei aerosols suppress precipitation, not only by inhibiting cloud-droplet coalescence into raindrops, but also by suppressing ice particle formation and thus cold-precipitation processes. The modeling case study of Li et al. (2009) conversely showed that increased smaller cloud condensation nuclei pollution aerosols produced 13% more precipitation in southern U.S. plains and more local intensive rainfall than with fewer aerosols.

b. Beijing urban climate

Beijing is one of the largest cities in the world, with exponential urban area and population growths since 1978, so that by 2012 it had 20.7 million residents. Beijing UHI studies have used data from its network

of Automatic Weather Station (AWS) sites, for example, with 20 sites, Lin and Yu (2005) showed its UHI increasing by 0.31°C decade^{-1} from 1960 to 2000. With 10 sites, Ji et al. (2006) found that the 1991–2000 UHI was stronger at night (0.84°C) than during the day (0.11°C),while one urban–rural station pair showed the 1977–2000 UHI most intense in winter (Liu et al. 2007). With 11 stations, Wang and Hu (2006) demonstrated that the 1993–2003 UHI expanded from the urban center to its outer suburbs, and that it exhibited a multicenter horizontal distribution over the city, dependent on the underlying land cover.

By 2013 more than 200 Beijing AWS sites existed, and thus Yang et al. (2013b) were able to investigate more detailed spatial and temporal features of the 2007–10 Beijing UHI by use of 56 urban and 8 rural stations. Maximum UHIs generally occurred in central urban areas, while smallest ones occurred in outer urban area. The largest and smallest seasonal-mean UHIs were 1.65°C for winter and 0.80°C for autumn, while the summer value was 0.9°C.

Relative humidity (RH) and vapor pressure (e) differences between one urban Beijing and one rural AWS site for the period 1971–2003 at 6-h intervals from 0200 local standard time (LST = UTC + 8 h) were studied by Liu et al. (2009). They found average climatological urban RH and e values always lower than rural values, with larger RH differences at 2000 and 0200 LST and larger e differences at 1400 and 2000 LST. Miao et al. (2010) observed (by use of 60 AWS sites) and simulated a Beijing UDI, however, during an August 2006 thunderstorm.

Analysis by Liu et al. (2006) of winds from 11 AWS sites during strong 1998–2003 summer UHIs showed convergence into urban Beijing. Miao and Chen (2008) and Miao et al. (2009) used both AWS data and modeling to show that local Beijing circulations are dominated by interactions between mountain valley winds and an UHI-induced circulation. Miao et al. (2010) likewise showed that the large Beijing roughness length z_0 reduces wind speed and that the urban area deflects 10-m winds.

Beijing AWS precipitation studies have provided insights into its impacts on precipitation; for example, Wu et al. (2000) showed increases in short-duration heavy precipitation both downwind of the city and in downtown Beijing, while Sun et al. (2006) found that a strong UHI initiated the heavy rain event in Beijing on 10 July 2004. Analysis of observed diurnal and spatial Beijing precipitation patterns by Yin et al. (2011), Wang et al. (2012), and Yang et al. (2013a) suggested that interactions between mountain–valley and land–sea breezes enhance UHI-induced convection.

Simulations with WRF by Miao et al. (2011) of the heavy regional rainfall around Beijing (during weak-UHI conditions) on 1 August 2006 showed that effects depended on the level of urbanization, as early urbanization (prior to 1980) decreased maximum rainfall over the city (because of increased surface drying), as compared with the no-urban simulation. Further modeled urbanization resulted additional decreases over the city due to a building-barrier bifurcation of precipitation, as storms were also diverted around the city.

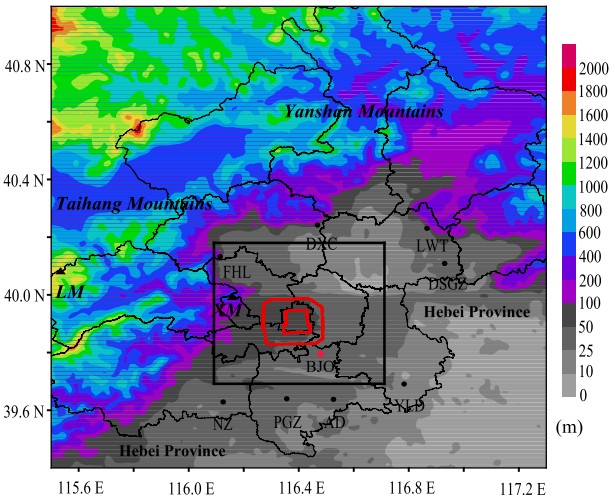

FIG. 1. Beijing area with topography (m; colors), city districts (gray lines), study area (black square), second and fourth RRs (inner and outer red outlined, respectively), Beijing Observatory (BJO; red dot), rural temperature stations (black dots), XM (white triangle), and Ling Mountain (LM; black triangle).

Whereas previous Beijing efforts have generally analyzed only one meteorological element, and usually with sparse observations, the current effort uses data from the now dense AWS network to determine interactions between detailed urban land use, temperature, specific humidity, wind direction and speed, and precipitation patterns over Beijing during summers from 2008 to 2012. It also represents the first test of the synthesis–hypothesis of Bornstein (2011), that is, that UHI intensity determines whether urban areas either initiate or enhance/bifurcate summer thunderstorms.

2. Methodology and data

Beijing is located in the north China plain (Fig. 1), east of the Taihang Mountains and south of the more distant Yanshan Mountains. The highest peak in the area (Wuling Mountain, not in figure) is about 100 km north of the urban center, with a height of about 2000 m above mean sea level (MSL); while Xiangshan Mountain (XM) is 25 km west of the city, but with a maximum height of only 500 m. The southeast plains occupy about 38% of the Beijing municipality, and that area has a temperate,

semihumid, continental monsoon climate, with hot summers, cold winters, and 80% of its precipitation in summer.

Beijing experienced rapid urbanization in recent decades, leading to rapid expansions in population and area. A transportation system consisting of multiple automobile ring roads (RRs) was developed in Beijing (Wang et al. 2010). The second RR (Fig. 1) opened in 1992, is 32.7 km in length, and encircles an area of about 62 km^2. The fourth RR opened in 2001, is 65.3 km in length, and is about 8 km from the city center. Areas within each RR have varied population and building densities (Yang et al. 2013b), with urban old town (OT) Beijing mainly within the second RR, and with newer denser taller areas between the second and fourth RRs (Fig. 2).

Analyses were thus carried out (in the black-box area in Fig. 1) into the detailed characteristics of meteorological elements in the Beijing urban area for the summers (June–August) of 2008–12. Rawinsonde data were collected at the Beijing Observatory (southern suburbs of Beijing, Fig. 1) and obtained from the National Meteorological Information Centre of the Beijing Meteorological Service, as were data from 64 AWS sites in and around central Beijing (Fig. 2).

All AWS data were quality controlled; that is, potentially erroneous values were removed based on the technique of Dou et al. (2008). Inclusion thresholds for 2-m temperature and relative humidity and for 10-m wind direction and speed were −80°–60°C, 0%–100%, 0°–360°, and 0–75 m s^{-1}, respectively. Extreme data (e.g., summer temperatures < 10°C, wind speed > 15 m s^{-1}, and hourly rainfall amounts > 50 mm) were checked by comparisons with adjacent sites. Stations with >5% missing values (of a particular meteorological parameter) were excluded from the analyses of that parameter. The number of AWS sites finally available for each meteorological parameter is shown in Table 1. Analyses were carried out for each AWS site separately to determine its average daytime (assumed to be 0800–1900 LST) and nighttime (assumed to be 2000–0700 LST) value of temperature, specific humidity, and wind speed over the study period following the techniques used in Miao et al. (2010) for determining spatial characteristics.

Near-surface flow-pattern types were classified by Cai et al. (2002) by use of diagnostic analysis, based on a mass-consistent wind field model and on observational data from 20 Beijing AWS sites during January, April, July, and October 1981. They found that 0200–0800 and 1200–2200 LST coincided with nighttime mountain-breeze and daytime valley-breeze periods, respectively, whereas 0900–1100 and 230–0100 LST were transitional periods. These daytime and nighttime periods were used for the analyses of wind direction, even though they do not exactly coincide with those (given above) for temperature, specific humidity, and wind speed. "Prevailing" station flow directions during the mountain- and valley-breeze periods were set to "modal" station directions.

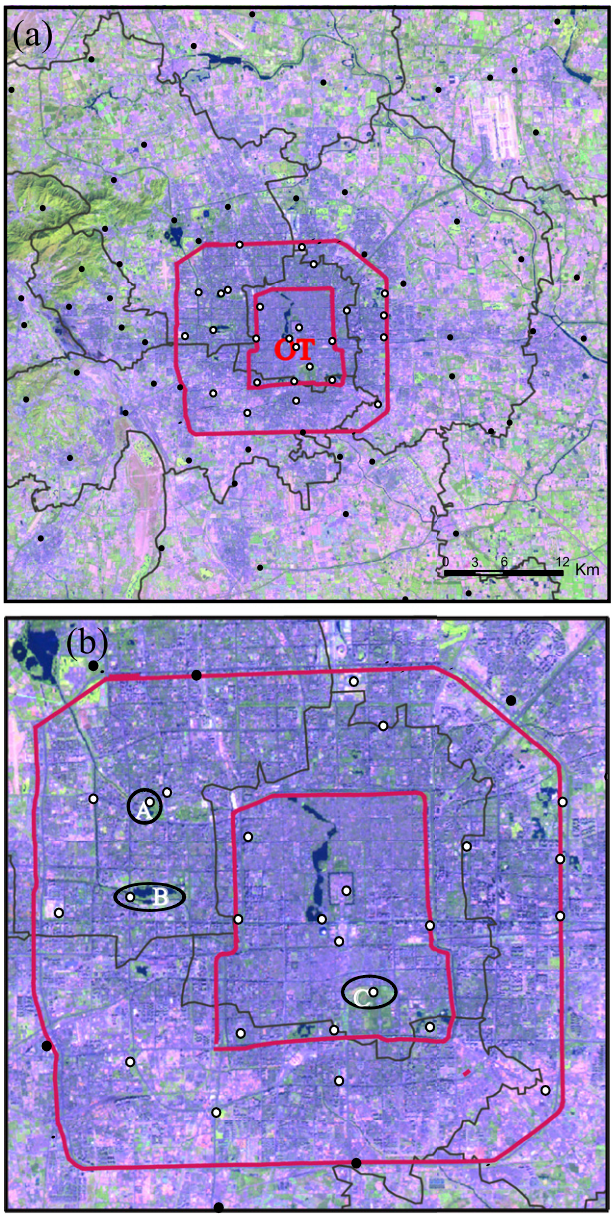

FIG. 2. Remote sensing images of the (a) study area, showing built-up areas (purple), green spaces (green), water bodies (blue), AWS sites (dots), OT, urban AWS sites (white dots), and rural AWS sites (black dots), and (b) magnified central (urban) area, showing green parks (black circles), i.e., Zizhuyuan (A), Yuyuantan (B), and Temple of Heaven (C).

Rawinsonde data were obtained from twice-daily launches (0800 and 2000 LST) during June and thrice-daily launches (0800, 1400, and 2000 LST) during July

TABLE 1. Numbers of AWS sites.

	Total	Used
Temperature	64	64
Specific humidity	47	44
Wind	55	53
Precipitation	64	64

and August. The 850-hPa wind velocity in the sounding prior to initiation of each rainfall event was defined as the low-level ''PBL wind.''

A rainfall event was defined as the concurrent occurrence of rain at least two AWS sites within the Beijing area, each with an hourly accumulation > 0.1 mm. A minimum of 3 h between events was required; 333 such events thus occurred between June and August during 2008–12. Each was classified according to the low-level PBL wind direction prior to the event. Southwesterly flows accounted for 134 cases (or 40% of all events), with southerly flows as the second most common (51 cases); the other directions accounted for only 14–33 cases each. To evaluate up- and downwind urban impacts on each storm, only southwesterly flow cases were studied.

Hourly average Beijing UHI intensity (UHII) was defined as follows:

$$\mathrm{UHII} = T_u - T_r, \tag{1}$$

where each hourly T_u value is the average of the hourly temperature values at all 26 urban stations within the fourth RR (Fig. 2a), while the corresponding T_r value is the average of only seven of the eight rural stations (Fig. 1), as values at DXC were missing for >5% of the study period (Yang et al. 2013b).

Each thunderstorm case was classified by its ''event'' UHII value (regardless of hour of occurrence), where an ''event'' UHII_j value (for event j) is defined as the maximum of the three pre-event hourly UHII values. The daily average 2008–12 Beijing summer UHII value was calculated herein as 1.25°C, and thus cases with an event $\mathrm{UHII}_j > 1.25$°C are hereinafter called strong-UHI events, while those with values below this threshold are called weak-UHI events.

Strong and weak UHII rainfall spatial distributions with thresholds of 1.0° and 1.5°C were similar to those with the 1.25°C threshold, and UHIs with a greater threshold do lead to greater rainfall impacts (not shown in section 3). This latter value was used as the criteria value, however, as it equaled the average (of daytime and nighttime) summer Beijing UHI value (as shown below in section 3). As expected from the previous Beijing studies discussed in section 1b, more than half (35 of 61) of the strong-UHI events occurred during nighttime (2000–0700 LST) hours, while most (53 of 73) of the weak-UHI events occurred during daytime (0800–1900 LST) hours.

Regional-normalized rainfall amount (NR) has been used in many studies (e.g., Yu. 2007), as it eliminates large-scale effects, thus highlighting local impacts; it is used in the current study and was calculated as follows:

$$R_i = \sum_j R_{i,j}, \tag{2}$$

$$\overline{R_i} = \frac{\sum_i^n R_i}{n}, \quad \text{and} \tag{3}$$

$$\mathrm{NR}_i = \frac{R_i - \overline{R_i}}{\overline{R_i}}, \tag{4}$$

where $R_{i,j}$ is rainfall at site i for event j, R_i is total study period rainfall at site i, $\overline{R_i}$ is study area average rainfall over the events of one case during the 2008–12 summers, and NR_i is its value at site i.

The Grid Analysis and Display System (GrADS) software program was used to create spatial isopleth patterns, but as it cannot fully account for the subtle topographic and urban distortions of most meteorological fields, additional subjective analysis was necessary (Lebassi et al. 2009). Adobe Illustrator was used to smooth final patterns, but no site value was ''violated'' during any step.

3. Results

a. Temperature

Mean nighttime (2000–0700 LST) summer temperatures (Fig. 3a) show expected low values in the western higher elevations. Urban values were closely correlated with underlying surfaces, which thus caused inhomogeneity; that is, industrial and densely populated high-rise urban regions (mainly between the second and fourth RRs) show higher values (maximum of 25.4°C), whereas the three green urban parks in Fig. 2b show low values.

The corresponding daytime pattern (0800–1900 LST, Fig. 3b) shows weaker gradients and the expected low values in the western higher elevations. The peak value (29.3°C) is now within the OT area (i.e., within the second RR), with relatively high values also near the eastern and southern edges of the fourth RR. Within the fourth RR, the maximum daytime difference between the downtown and its green parks was 2.0°C, whereas during the nighttime it was only 1.0°C.

Spatial distributions of period-average daytime and nighttime temperature differences between each study

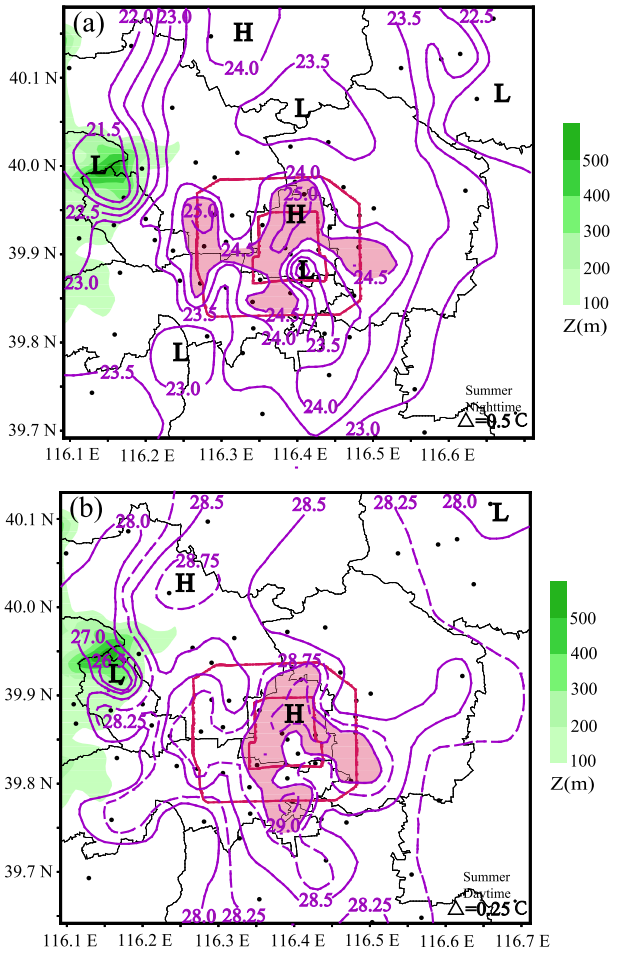

FIG. 3. Average 2008–12 summer Beijing urban area: (a) nighttime (2000–0700 LST) and (b) daytime (0800–1900 LST) 2-m temperatures (°C), both with second and fourth RRs (red outlined areas), terrain heights (m; green shading), high (H) and low (L) temperature areas, and high urban values (purple shading). Note the smaller temperature contour gradient in the daytime.

area site and the corresponding period-average T_r value [i.e., average of the seven rural stations, as in Eq. (1)] were calculated. The maximum difference (not shown) was 1.4°C during the day and 5.3°C at night. For comparison, the average UHII (defined in section 2) was 1.7°C at night and 0.8°C during the day, while the daily average was 1.25°C (also selected as the weak–strong UHII threshold of the current thunderstorm analysis, as discussed above in section 2).

By use of stations inside sixth RR as urban sites Yang et al. (2013b) found a summer daily average UHI value (for 2007–10 vs the 2008–12 period of the current study) of 0.9°C. This value is about 27% lower than the 1.25°C daily average UHII value of the current study, as the predominant land cover between fourth and sixth RR is cropland, while the urban stations of the current study are in the more built-up areas within fourth RR (as discussed in section 2).

The (wet season) summer Beijing UHIs are strongest at night, consistent with the theory of Swaid (1991) and Imamura (1991), as described in section 1a; that is, urban building materials warm more rapidly during daytime hours and cool more rapidly during nighttime hours than do wet rural soils. High urban buildings also produce stronger nocturnal UHIs, as their large heat capacity trap and store solar energy during the day (thus keeping 2-m urban temperatures low), but slowly release it at night (thereby keeping 2-m urban temperatures warm). The high buildings in the built-up areas between the second and fourth RRs thus show the peak nighttime 2-m UHIs, while peak daytime values conversely occur in the less urbanized OT area.

b. *Specific humidity*

Mean nighttime (2000–0700 LST) specific humidity (Fig. 4a) shows an average of 14.1 g kg^{-1}, again with an inhomogeneous distribution, with low values again related to higher elevations. Low values (minimum of 13.3 g kg^{-1}) are also found near urban centers (between the second and fourth RRs), as compared to those in sparse building, green, and water areas; the maximum UDI magnitude (urban minimum minus rural maximum) is −2.4 g kg^{-1}.

The mean daytime (0800–1900 LST) pattern (Fig. 4b) is similar to that during night, but with a slightly lower average of 13.8 g kg^{-1}. The minimum value (12.8 g kg^{-1}) is again near the western edge of the second RR, but relatively low levels (12.9 g kg^{-1}) are also found near the western and eastern edges of the fourth RR; the maximum UDI (urban minimum minus rural maximum) is only −1.9 g kg^{-1}.

Daytime urban effects on specific humidity are multiple; for example, combustion releases water vapor into the urban PBL, but vegetation is replaced by concrete and asphalt, thereby decreasing evapotranspiration and increasing runoff, and thus lowering urban specific humidity levels. Warmer urban daytime PBLs are also more convective than rural PBLs, increasing upward-directed urban moisture fluxes, and thus making urban daytime specific humidity lower than nearby rural values (Chen 1997).

Temperature and specific humidity urban impacts are generally inversely related in most of the study area (Figs. 3 and 4), but air near the eastern edge of the fourth RR is both hot and wet during day and night. One explanation for this could be the cogeneration energy plant near its observation station, which produces drainage water with temperatures up to 40°C.

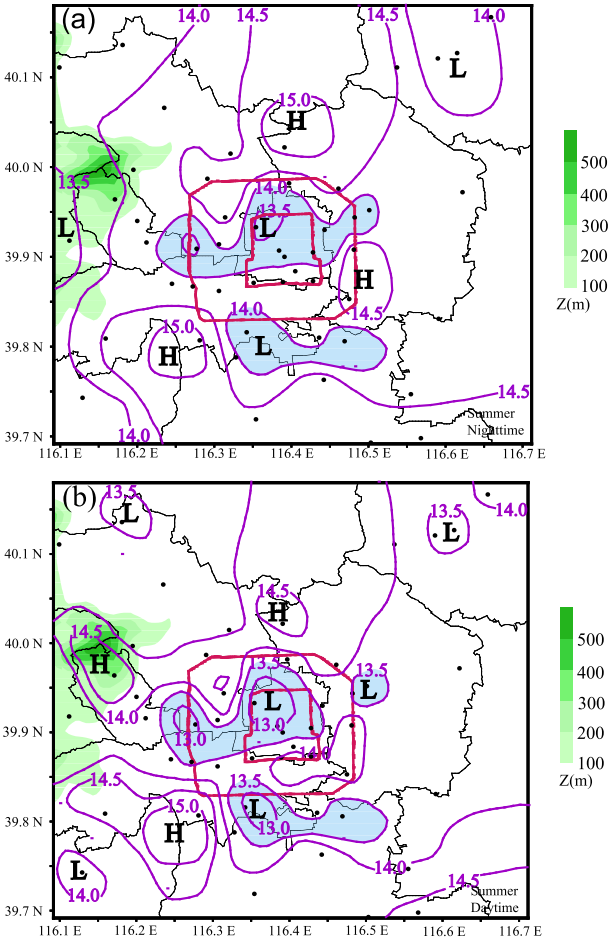

FIG. 4. As in Fig. 3, but for specific humidity (g kg^{-1}), and with low-value urban areas (blue) shaded.

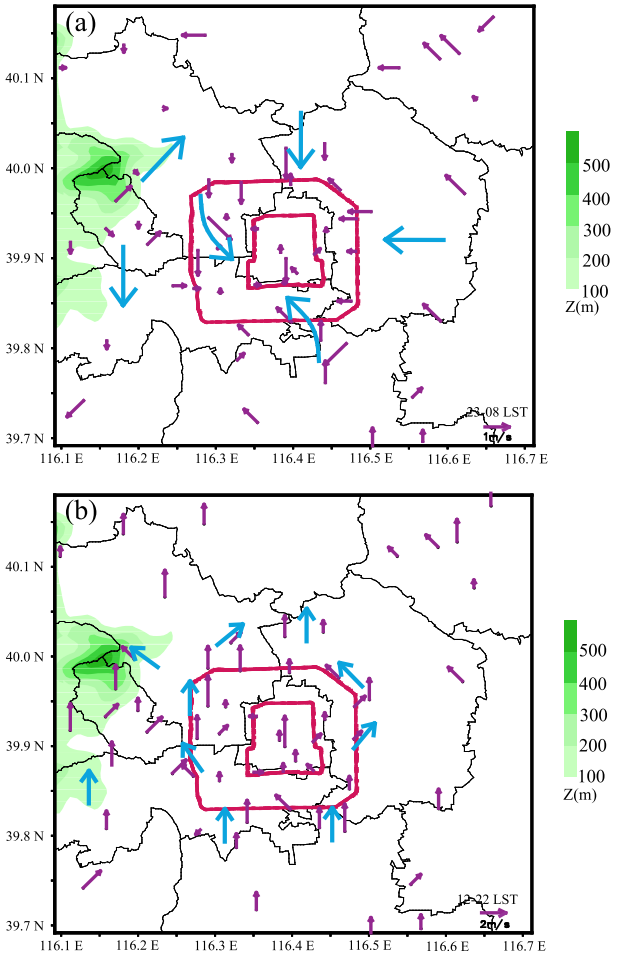

FIG. 5. As in Fig. 3, but for prevailing wind direction during (a) 0200–0800 and (b) 1200–2200 LST; blue arrows represent subjective space average flow directions.

c. *Wind direction*

Beijing area prevailing large-scale low-level flows are southerly (Cai et al. 2002), but prevailing summer nighttime (0200–0800 LST) winds show downslope mountain breezes (from the hills toward the urban center) in western and northern areas (Fig. 5a). As Beijing UHIs are strongest at night (Fig. 3a), resulting UHI-induced convergence into the city augments the mountain breeze. Daytime (1200–2200 LST) flows in the western and northern portions of the study area are reversed, with upslope flows directed toward mountain peaks (Fig. 5b) and not impacting the city. As daytime Beijing UHIs are relatively weak (Fig. 3b), a dominant UHI-induced convergence does not develop, but a tendency for an urban-scale building-barrier-induced divergence is seen (consistent with Bornstein 2011).

The blue arrows in both figures are subjective "gross" average in-space flow directions, which cannot thus "represent" every direction in the areas through which they are drawn. Sites in the OT urban center (within or near the second RR) probably are influenced by local building distributions; for example, the high-speed value in the center of ring 2 is in the center of the Forbidden City, which has only a few scattered low-rise buildings.

d. *Wind speed*

Nighttime (0200–0800 LST) average speeds across the region (Fig. 6a) are extremely low, but with expected peak values (>1.5 m s^{-1}) in high-altitude mountain regions, and with a minimum (<0.3 m s^{-1}) in the northwest domain edge. Speeds within the urban area show an interesting pattern, with high speeds (>1.5 m s^{-1}) at three locations outside the fourth RR, low speeds (<0.6 m s^{-1}) between it and the second RR, and moderate speeds (peak > 0.9 m s^{-1}) in the OT area within the second RR.

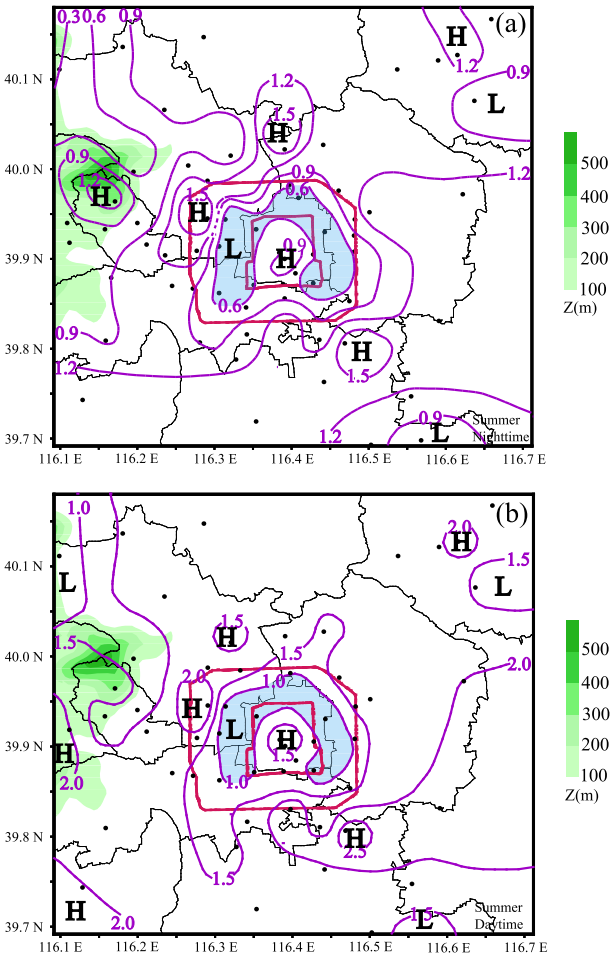

FIG. 6. As in Fig. 4, but for wind speed ($m\,s^{-1}$) and with low-speed areas shaded (blue). Note the larger wind speed contour gradient in the daytime.

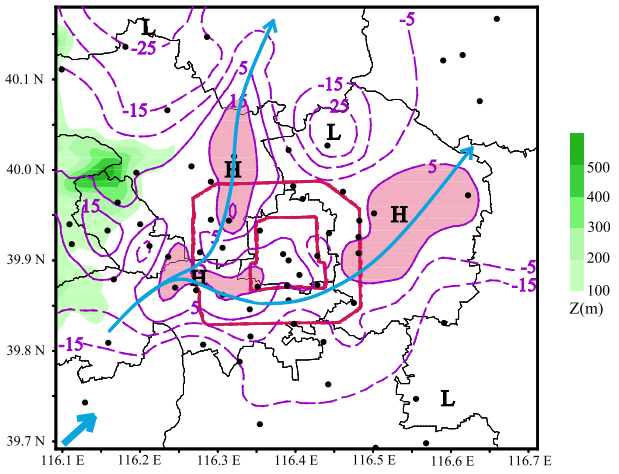

FIG. 7. As in Fig. 3, but for normalized total rainfall amounts (%) for all cases with 850-hPa winds from southwest. High urban precipitation areas are shaded (red), and the blue arrows show a bifurcating streamline.

The explanation for this urban pattern is found in the numerical model results of Bornstein (1975), which simulated flows over a rough heated city; that is, flows initially accelerated inward toward the city because of UHI-induced convergence (as in Fig. 3a), but then decelerate when they encounter the high-z_0 urban edge (outer boundary of fourth RR), as z_0 deceleration is stronger there than is the UHI-induced acceleration. Speeds increase again, as convergence-induced acceleration overcomes z_0 deceleration, as the flow enters into the small building area in the OT city center. The maximum difference between the OT maximum speed and the lowest value is $1.3\,m\,s^{-1}$.

Daytime (1200–2200 LST) average wind speeds across the region (Fig. 6b) are somewhat higher (average of 1.5 vs $1.0\,m\,s^{-1}$) as expected, as increased vertical mixing increases downward momentum fluxes. The western high-altitude regions thus show higher values ($>1.8\,m\,s^{-1}$) and a higher minimum ($<0.9\,m\,s^{-1}$) exists at the northwest domain edge. Speeds within the urban area also show the nighttime pattern, but with also higher values for the speed peak ($>2.4\,m\,s^{-1}$) outside the fourth RR, the minimum ($<0.9\,m\,s^{-1}$) between it and the second RR, and the OT moderate peak ($>1.5\,m\,s^{-1}$). The maximum difference between the OT peak and the lowest speed is also slightly larger than during the nighttime period (1.6 vs $1.3\,m\,s^{-1}$).

e. Precipitation

Overall (regardless of time of day and of event UHI magnitude, as defined in section 2) regional NR values (Fig. 7) under the most prevalent 850-hPa regional flow direction (i.e., southwesterly) are partly controlled by terrain effects, for example, the strong rain shadow ($<-25\%$) downwind of the western mountains. The three urban-related maxima (one up to 15%) are, however, consistent with storm bifurcation impacts from a building-barrier effect, as are both the resulting weak OT minimum and strong rain-shadow effect ($>-25\%$) directly downwind of the urban area; this latter magnitude equals the similar topographic shadow.

When these total NR results are segmented by event UHII magnitude (again regardless of time of day), the weak-UHI cases (Fig. 8a) now show an even greater urban barrier-induced impact, that is, both western maxima are now >15%, while both the OT minimum ($>-15\%$) and urban rain shadow ($>-35\%$) have thus intensified. This is consistent with the urban-barrier part of the urban precipitation synthesis–hypothesis of Bornstein (2011) discussed in section 1a and shows that the barrier bifurcation cases dominate the UHI-initiated cases in this study.

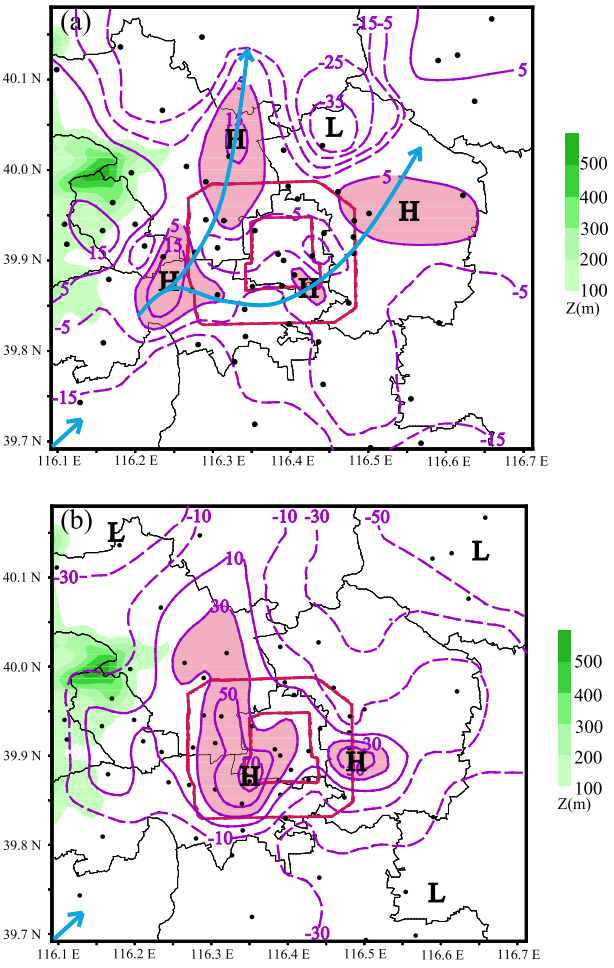

FIG. 8. As in Fig. 7, but for (a) weak- and (b) strong-UHI cases. Note the stronger contour gradient in the strong-UHI case.

The corresponding NR values for the strong-UHI cases (Fig. 8b) do not show barrier-induced impacts, however, but instead show two UHI-induced urban maximum (60% and 75%) generally in the most urbanized area (i.e., between the second and fourth RRs). This UHI-induced convection is also consistent with the second part of the Bornstein (2011) hypothesis. Note that study area average rainfall $\overline{R_i}$ under southwest winds with weak UHIs (527 mm) is larger (as expected) than with strong UHIs (178 mm), as weak UHIs occur with regionwide storms, while strong UHIs form with clear-sky localized urban-induced storms.

4. Conclusions

The study analyzed twice- or thrice-daily rawinsonde observations and hourly meteorological measurements collected during summer (June–August) of 2008–12 from a dense surface network in the Beijing area. The data were used to determine spatial characteristics of 2-m temperature and specific humidity, 10-m wind speed and direction, and precipitation amount, and to assess Beijing urban climate impacts on these parameters during daytime and nighttime hours.

Results showed Beijing nighttime UHI values stronger than daytime values (1.7° vs 0.8°C, respectively), with both showing multicenter distributions related to urban land-use patterns. Maximum nighttime temperatures were mainly within the industrial and densely populated high-rise urban regions between the second and fourth ring roads, whereas urban parks showed low values. Daytime maximum UHIs were within the Beijing OT region (i.e., within the second RR).

Daytime and nighttime Beijing specific humidity values were lower than in surrounding regions, with stronger urban dry island intensity during daytime than nighttime (maximum of -2.4 vs $-1.9\,\mathrm{g\,kg^{-1}}$). Values again showed a multicenter distribution due to the nonuniform distribution of nonevaporating urban impervious surfaces, which decrease evapotranspiration and increase runoff, and thus lower urban specific humidity levels. Warm urban daytime PBLs are also more convective than rural PBLs, which increased upward-directed moisture fluxes, making urban daytime specific humidity lower than nearby rural values.

Early morning low-level winds converged into the Beijing area because of a combination of downslope mountain breezes and strong-UHI-induced convergence. The weaker afternoon and evening upslope valley breezes did not impact the urban area, and the now-weaker UHI also did not produce convergence into the city. The regional flow, however, was bifurcated around the city by its now-dominant urban-barrier effect.

Regional early morning flows that approached the city first accelerate inward towards its center because of UHI-induced convergence but then decelerated because of its high urban z_0, resulting in low speeds in the dense built-up area between the second and fourth RRs. Speeds again increased, as the flow entered the small building area in the OT city center, as convergence-induced acceleration overcame z_0 deceleration.

Regional daytime speeds are only somewhat higher than nighttime values (average of 1.5 vs $1.0\,\mathrm{m\,s^{-1}}$), as increased vertical mixing increase downward momentum fluxes. Urban daytime speeds show the same pattern as above, but with thus slightly higher values. The maximum daytime difference between the OT high speed and the lowest value is slightly larger (1.6 vs $1.3\,\mathrm{m\,s^{-1}}$) than the nighttime value. These results are consistent with those of Bornstein and Johnson (1977), who showed that both daytime and nighttime wind speeds through NYC were accelerated by UHIs (during periods with slow background regional

flows) and both were decelerated (during periods with fast background regional flows) by the larger urban z_0 values.

Overall regional-normalized total rainfall values under the most prevalent 850-hPa regional flow direction (i.e., southwesterly) are mainly controlled by terrain and urban-barrier effects; for example, a strong rain shadow ($<-25\%$) exists downwind of the western mountains. Urban-related maximum (on its lateral boundaries, and up to 15%) are consistent with storm-bifurcation impacts from building-barrier effects, as are both the resulting weak OT minimum and strong rain shadow effect ($>-25\%$) directly downwind of the urban area.

When the total NR results are segmented by event UHI magnitude (regardless of time of day), the weak-UHI (<1.25°C) cases show greater urban-barrier-induced impacts, that is, lateral maximum increased to >15%, while both the OT minimum ($>-15\%$) and urban rain shadow ($>-35\%$) also intensified. The strong-UHI (>1.25°C) cases, however, did not show barrier-induced impacts, but instead displayed two UHI-induced urban maxima (60%–75%) in the most urbanized area (i.e., between the second and fourth RRs). Study area average rainfall during the prevailing southwesterly flow cases with weak UHIs was larger (as expected) than with strong UHIs (527 vs 178 mm), as weak UHIs occur with regionwide storms, but strong UHIs form with clear-sky conditions and can thus produce localized urban-induced storms.

In contrast to prior studies (e.g., Shepherd et al. 2002; Burian and Shepherd 2005), the current manuscript does not show (regardless of UHI magnitude) increased precipitation directly downwind of the city, although in weak-UHI cases, areas with maximum precipitation exist, but only on its downwind lateral corners. This apparent inconsistency may result, as this study examined the precipitation pattern in downwind areas in a more spatially detailed manner.

In summary, climatological–statistical analyses of concurrent Beijing summer daytime and nighttime urban climate impacts on the spatial distributions of temperature, specific humidity, wind direction, and wind speed have allowed for determination of interactions between these parameters, as well as their impacts on summer thunderstorm convective precipitation. Results show that low-speed, strong-UHI conditions (mainly at night) produced inward-directed urban convergent flows, which trigger convective (or perhaps even intensify existing storms advected into a strong UHI) thunderstorms and maximized their precipitation over Beijing, even as its specific humidity levels are less than in surrounding areas, as the moisture in these storms is advected into the city by UHI-induced convergent flows.

Unpublished reinterpretation (by the authors of the current effort) of the case-study simulations of Miao et al. (2011) seem to indicate that an existing storm was in fact drawn into the Beijing UHI, intensified, trapped, and ultimately dissipated over the city. Such a phenomenon would extend the Bornstein (2011) hypothesis–synthesis and thus requires further study.

Results also show that higher-speed, weak-UHI conditions (mainly during daytime hours) produced both flow and thunderstorm bifurcation around Beijing. This effect thus minimized precipitation over and downwind of the city, but produced areas of maximum precipitation on its downwind lateral boundaries. To properly define upwind, downwind, and lateral areas in a climatological study seeking to understand urban thermodynamic impacts on precipitation, it is necessary to segment moving storms by their direction of movement, and thus in the current study only considered the most common case of storms moving to the city from the southwest.

These precipitation results are consistent with the synthesis–hypothesis of Bornstein (2011) concerning urban impacts on summertime convective thunderstorm dynamics. The current study, however, goes deeper into this synthesis; that is, the older study did segment initiated vs bifurcated thunderstorm cases, but it only hypothesized that UHI magnitude was the controlling parameter. The current study, however, determined that a critical UHI magnitude of 1.25°C segmented the initiated cases (associated with UHI values above this threshold) from the bifurcated cases (associated with smaller UHI values); this study thus represents the first validation of the synthesis–hypothesis. Analysis showed that the daily average UHI during the study period was in fact 1.25°C, and thus this value was used as the segmentation criteria, even though larger values (and thus fewer cases) showed stronger downwind urban induced precipitation reductions.

These results are scientifically important, as they provide the first detailed comprehensive study of the spatial distributions of daytime and nighttime summer Beijing impacts (and interactions) on temperature, specific humidity, wind velocity, and precipitation. Summer heat waves and urban thunderstorm-induced flooding produce large losses in human life and infrastructure, and thus these results will be useful in the planning to improve the lived-in environment and in disaster prevention and mitigation in a changing climate.

Although this study used a denser Beijing AWS network than all previous such studies, additional sites would produce even deeper insights into the distribution of its local-scale urban climate impacts. As only summer thunderstorms were considered, additional seasons and precipitation mechanisms (e.g., synoptic fronts) need analysis. All the physical mechanisms by which cities alter precipitation patterns have also not been completely

examined; for example, aerosol impacts on Beijing precipitation, shown to be significant (Duan and Mao 2009), were not considered.

Future efforts should include both climatological and short-term intensive field studies, complete with PBL observations from sodars, lidars, radars, towers, satellites, aircraft, and helicopters (Chen et al. 2012). Future numerical simulations should be carried out with the NCAR highly urbanized version of WRF (Chen et al. 2011) and with a focus on urban aerosol impacts and on urban mechanisms that bifurcate moving thunderstorms.

Such storms (less frequently) bifurcate over the U.S. Great Plains in the presence of anticyclonic vertical wind shears; and perhaps the more frequent urban bifurcation is related to anticyclonic turning (toward low pressure) of urban PBL flows due to wind speed reductions, as flows enter urban areas (with their higher z_0 values). Another explanation for bifurcation could be the possible formation of an area of high pressure, associated with urban-induced upwind downward motions that form to compensate for mass redistributions associated with urban-induced upward motions over city centers.

Acknowledgments. The authors thank Lin Li and Jiqin Zhong for providing the data used in the study. This work was supported by National Natural Science Foundation of China (Grant 41175015), Beijing Natural Science Foundation (Grant 8122022), and Beijing Municipal Science and Technology Commission (Grant Z111100074211010).

REFERENCES

Ackerman, B., 1971: Moisture content of city and country air. Preprints, *Conf. on Air Pollution Meteorology,* Raleigh, NC, Amer. Meteor. Soc., 154–158.

Atkinson, B. W., 1985: *The Urban Atmosphere.* Cambridge University Press, 89 pp.

Bornstein, R. D., 1968: Observations of the urban heat island effect in New York City. *J. Appl. Meteor.,* **7,** 575–582, doi:10.1175/1520-0450(1968)007<0575:OOTUHI>2.0.CO;2.

——, 1975: The two-dimensional URBMET urban boundary layer model. *J. Appl. Meteor.,* **14,** 1459–1477, doi:10.1175/1520-0450(1975)014<1459:TTDUUB>2.0.CO;2.

——, 2011: Establishment of meso-met modeling case studies to evaluate the relative roles of urban dynamics and aerosols on summer thunderstorms: A proposal. *18th Conf. on Planned and Inadvertent Weather Modification, and Third Symp. on Aerosol–Cloud–Climate Interactions,* Seattle, WA, Amer. Meteor. Soc., J5.2. [Available online at https://ams.confex.com/ams/91Annual/recordingredirect.cgi/id/17137.]

——, and D. S. Johnson, 1977: Urban-rural wind velocity differences. *Atmos. Environ.,* **11,** 597–604, doi:10.1016/0004-6981(77)90112-3.

——, and G. LeRoy, 1990: Urban barrier effects on convective and frontal thunderstorms. Preprints, *Fourth Conf. on Mesoscale Processes,* Boulder, CO, Amer. Meteor. Soc., 120–121.

——, and Q. Lin, 2000: Urban heat islands and summertime convective thunderstorms in Atlanta: Three case studies. *Atmos. Environ.,* **34,** 507–516, doi:10.1016/S1352-2310(99)00374-X.

——, R. Imamura, J. E. González, and B. Lebassi, 2012: Interactions of global-warming and urban heat islands in different climate-zones. *National Security and Human Health Implications of Climate Change,* H. Fernando et al., Eds., NATO Science for Peace and Security Series C: Environmental Security, Springer, 49–60.

Brazel, A., N. Selover, R. Vose, and G. Heisler, 2000: The tale of two climates—Baltimore and Phoenix urban LTER sites. *Climate Res.,* **15,** 123–135, doi:10.3354/cr015123.

Burian, S. J., and J. M. Shepherd, 2005: Effect of urbanization on the diurnal rainfall pattern in Houston. *Hydrol. Processes,* **19,** 1089–1103, doi:10.1002/hyp.5647.

Cai, X., Y. Guo, H. Liu, and J. Chen, 2002: Flow pattern of lower atmosphere over Beijing area (in Chinese with English abstract). *Acta Sci. Nat. Univ. Pekin.,* **38,** 387–392.

Chen, F., and Coauthors, 2011: The integrated WRF/urban modelling system: Development, evaluation, and applications to urban environmental problems. *Int. J. Climatol.,* **31,** 273–288, doi:10.1002/joc.2158.

——, and Coauthors, 2012: Research priorities in observing and modeling urban weather and climate. *Bull. Amer. Meteor. Soc.,* **93,** 1725–1728, doi:10.1175/BAMS-D-11-00217.1.

Chen, Q., 1997: The influence of urbanization on climate in Fuzhou city (in Chinese with English abstract). *Meteor. Mon.,* **23,** 41–45.

Clark, E. C., R. Bornstein, and Y. T. Tam, 1985: Current and potential anthropogenic moisture effects on the NYC planetary boundary layer. *J. Air Pollut. Control Assoc.,* **35,** 831–835, doi:10.1080/00022470.1985.10465963.

Craig, K., and R. Bornstein, 2002: MM5 simulations of urban induced convective precipitation over Atlanta. Preprints, *Fourth Conf. on the Urban Environment,* Norfolk, VA, Amer. Meteor. Soc., 1.3. [Available online at https://ams.confex.com/ams/AFMAPUE/techprogram/paper_38803.htm.]

Dou, Y., Y. S. Tao, and B. Hu, 2008: The application of quality control procedures for real-time data form automatic weather stations (in Chinese with English abstract). *Meteor. Mon.,* **34,** 77–81.

Duan, J., and J. Mao, 2009: Influence of aerosol on regional precipitation in north China. *Chin. Sci. Bull.,* **54,** 474–483, doi:10.1007/s11434-008-0447-6.

Fujibe, F., 2003: Long-term surface wind changes in the Tokyo metropolitan area in afternoon of sunny days in the warm season. *J. Meteor. Soc. Japan,* **81,** 141–149, doi:10.2151/jmsj.81.141.

Garstang, M., P. Tyson, and G. Emmitt, 1975: The structure of heat islands. *Rev. Geophys.,* **13,** 139–165, doi:10.1029/RG013i001p00139.

Georgescu, M., M. Moustaoui, A. Mahalov, and J. Dudhia, 2011: An alternative explanation of the semiarid urban area "oasis effect." *J. Geophys. Res.,* **116,** D24113, doi:10.1029/2011JD016720.

——, ——, ——, and ——, 2012: Summer-time climate impacts of projected megapolitan expansion in Arizona. *Nat. Climate Change,* **3,** 37–41, doi:10.1038/nclimate1656.

Hage, K., 1975: Urban–rural humidity differences. *J. Appl. Meteor.,* **14,** 1277–1283, doi:10.1175/1520-0450(1975)014<1277:URHD>2.0.CO;2.

Hjelmfelt, M. R., 1982: Numerical simulation of the effects of St. Louis on mesoscale boundary-layer airflow and vertical air motion: Simulations of urban vs. nonurban effects. *J. Appl. Meteor.,* **21,** 1239–1257, doi:10.1175/1520-0450(1982)021<1239:NSOTEO>2.0.CO;2.

Howard, L., 1833: *The Climate of London, Deduced from Meteorological Observations, Made in the Metropolis, and at Various Places around It*. 3rd ed. Vol. 1, Harvey and Dorton, 348 pp.

Huff, F., and S. Changnon Jr., 1972: Climatological assessment of urban effects on precipitation at St. Louis. *J. Appl. Meteor.,* **11,** 823–842, doi:10.1175/1520-0450(1972)011<0823:CAOUEO>2.0.CO;2.

——, and ——, 1973: Precipitation modification by major urban areas. *Bull. Amer. Meteor. Soc.,* **54,** 1220–1225, doi:10.1175/1520-0477(1973)054<1220:PMBMUA>2.0.CO;2.

Imamura, I. R., 1991: Observational studies of urban heat island characteristics in different climate zones. Ph.D. thesis, University of Tsukuba, 145 pp.

Jauregui, E., 1997: Heat island development in Mexico City. *Atmos. Environ.,* **31,** 3821–3831, doi:10.1016/S1352-2310(97)00136-2.

Ji, C., W. Liu, and C. Xuan, 2006: Impact of urban growth on the heat island in Beijing (in Chinese with English abstract). *Chin. J. Geophys.,* **49,** 69–77.

Jin, M., R. E. Dickinson, and D. Zhang, 2005: The footprint of urban areas on global climate as characterized by MODIS. *J. Climate,* **18,** 1551–1565, doi:10.1175/JCLI3334.1.

Kim, Y. H., and J. J. Baik, 2005: Spatial and temporal structure of the urban heat island in Seoul. *J. Appl. Meteor.,* **44,** 591–05, doi:10.1175/JAM2226.1.

Landsberg, H. E., 1981: *The Urban Climate.* Academic Press, 234 pp.

Lebassi, B., J. Gonzalez, D. Fabris, E. Maurer, N. Miller, C. Milesi, P. Switzer, and R. Bornstein, 2009: Observed 1970–2005 cooling of summer daytime temperatures in coastal California. *J. Climatol.,* **22,** 3558–3573, doi:10.1175/2008JCLI2111.1.

Li, G., Y. Wang, K.-H. Lee, Y. Diao, and R. Zhang, 2009: Impacts of aerosols on the development and precipitation of a mesoscale squall line. *J. Geophys. Res.,* **114,** D17205, doi:10.1029/2008JD011581.

Lin, X., and S. Yu, 2005: Interdecadal changes of temperature in the Beijing region and its heat island effect (in Chinese with English abstract). *Chin. J. Geophys.,* **48,** 47–54, doi:10.1002/cjg2.624.

Liu, W., C. Ji, J. Zhong, X. Jiang, and Z. Zheng, 2007: Temporal characteristics of the Beijing urban heat island. *Theor. Appl. Climatol.,* **87,** 213–221, doi:10.1007/s00704-005-0192-6.

——, H. You, and J. Dou, 2009: Urban–rural humidity and temperature differences in the Beijing area. *Theor. Appl. Climatol.,* **96,** 201–207, doi:10.1007/s00704-008-0024-6.

Liu, X., F. Hu, and L. Li, 2006: Analyses on the characteristics of Beijing summer urban heat island (UHI) and its meteorological fields (in Chinese with English abstract). *J. Grad. Sch. Chin. Acad. Sci.,* **23,** 70–76.

Magee, N., J. Curtis, and G. Wendler, 1999: The urban heat island effect at Fairbanks, Alaska. *Theor. Appl. Climatol.,* **64,** 39–47, doi:10.1007/s007040050109.

Manley, G., 1958: On the frequency of snowfall in metropolitan England. *Quart. J. Roy. Meteor. Soc.,* **84,** 70–72, doi:10.1002/qj.49708435910.

Miao, S., and F. Chen, 2008: Formation of horizontal convective rolls in urban areas. *Atmos. Res.,* **89,** 298–304, doi:10.1016/j.atmosres.2008.02.013.

——, ——, M. A. LeMone, M. Tewari, Q. Li, and Y. Wang, 2009: An observational and modeling study of characteristics of urban heat island and boundary layer structures in Beijing. *J. Appl. Meteor. Climatol.,* **48,** 484–501, doi:10.1175/2008JAMC1909.1.

——, ——, Q. Li, and S. Fan, 2010: Month averaged impacts of urbanization on atmospheric boundary layer structure and precipitation in summer in Beijing area (in Chinese with English abstract). *Chin. J. Geophys.,* **53,** 1580–1593.

——, ——, ——, and ——, 2011: Impacts of urban processes and urbanization on summer precipitation: A case study of heavy rainfall in Beijing on 1 August 2006. *J. Appl. Meteor. Climatol.,* **50,** 806–825, doi:10.1175/2010JAMC2513.1.

Oke, T., 1987: *Boundary Layer Climates.* Academic Press, 345 pp.

Ripley, E., O. Archibold, and D. Bretell, 1996: Temporal and spatial temperature patterns in Saskatoon. *Weather,* **51,** 398–405, doi:10.1002/j.1477-8696.1996.tb06171.x.

Rosenfeld, D., 2000: Suppression of rain and snow by urban and industrial air pollution. *Science,* **287,** 1793–1806, doi:10.1126/science.287.5459.1793.

Seto, K. C., M. Fragkias, B. Guneralp, and M. K. Reilly, 2011: A meta-analysis of global urban land expansion. *PLoS ONE,* **6,** e23777, doi:10.1371/journal.pone.0023777.

Shem, W., and M. Shepherd, 2009: On the impact of urbanization on summertime thunderstorms in Atlanta: Two numerical model case studies. *J. Atmos. Res.,* **92,** 172–179, doi:10.1016/j.atmosres.2008.09.013.

Shepherd, J. M., 2005: A review of current investigations of urban-induced rainfall and recommendations for the future. *Earth Interact.,* **9,** 1–27, doi:10.1175/EI156.1.

——, H. Pierce, and A. J. Negri, 2002: Rainfall modification by major urban areas: Observations from spaceborne rain radar on the TRMM satellite. *J. Appl. Meteor.,* **41,** 689–701, doi:10.1175/1520-0450(2002)041<0689:RMBMUA>2.0.CO;2.

Stewart, I. D., and T. R. Oke, 2012: Local climate zones for urban temperature studies. *Bull. Amer. Meteor. Soc.,* **93,** 1879–1900, doi:10.1175/BAMS-D-11-00019.1.

Sun, J., H. Wang, L. Wang, F. Liang, Y. Kang, and X. Jiang, 2006: The role of urban boundary layer in local convective torrential rain happening in Beijing on 10 July 2004 (in Chinese with English abstract). *Chin. J. Atmos. Sci.,* **30,** 221–234.

Swaid, H., 1991: Nocturnal variation of air–surface temperature gradients for typical urban and rural surfaces. *Atmos. Environ.,* **25B,** 333–341, doi:10.1016/0957-1272(91)90005-Y.

Unkašević, M., O. Jovanović, and T. Popović, 2001: Urban–suburban/rural vapour pressure and relative humidity differences at fixed hours over the area of Belgrade city. *Theor. Appl. Climatol.,* **68,** 67–73, doi:10.1007/s007040170054.

Wang, J., R. Zhang, and Y. Wang, 2012: Areal differences in diurnal variations in summer precipitation over Beijing metropolitan region. *Theor. Appl. Climatol.,* **110,** 395–408, doi:10.1007/s00704-012-0636-8.

Wang, X., X. Li, and Z. Feng, 2010: Research on urban extension based on Shannon entropy (in Chinese with English abstract). *China Popul. Resour. Environ.,* **20,** 88–2.

Wang, Y., and F. Hu, 2006: Variations of the urban heat island in summer of the recent 10 years over Beijing (in Chinese with English abstract). *Chin. J. Geophys.,* **49,** 61–68.

Wu, X., X. Wang, X. Zeng, and L. Xu, 2000: The effect of urbanization on short duration precipitation in Beijing (in Chinese with English abstract). *J. Nanjing Inst. Meteor.,* **23,** 68–72.

Yang, P., G. Ren, W. Hou, and W. Liu, 2013a: Spatial and diurnal characteristics of summer rainfall over Beijing Municipality based on a high-density AWS dataset. *Int. J. Climatol.,* **33,** 2769–2780, doi:10.1002/joc.3622.

——, ——, and W. Liu, 2013b: Spatial and temporal characteristics of Beijing urban heat island intensity. *J. Appl. Meteor. Climatol.,* **52,** 1803–1816, doi:10.1175/JAMC-D-12-0125.1.

Yin, S., W. Li, D. Chen, and J.-H. Jeong, 2011: Diurnal variations of summer precipitation in the Beijing area and the possible effect of topography and urbanization. *Adv. Atmos. Sci.,* **28,** 725–734, doi:10.1007/s00376-010-9240-y.

Yu, Q., 2007: Inter-annual variability of precipitation urbanization effects in Beijing. *Prog. Nat. Sci.,* **17,** 632–638.